

Addition Coupled Electron Transfer (ACET) and Addition Coupled Electron Coupled Proton Transfer (ACPCET)

Yumiao Ma^{*a,b}

- a. BSJ Institute, Haidian, Beijing, 100084, People's Republic of China. ymma@bsj-institute.top
- b. Hangzhou Yanqu Information Technology Co., Ltd. Xihu District, Hangzhou City, Zhejiang Province, 310003, People's Republic of China

Abstract: The new types of elementary reaction in which a nucleophilic addition (A) to quinones is coupled with electron transfer (ET) and even further proton transfer (PT) are suggested herein by density functional theory calculation, which are called Addition Coupled Electron Transfer (ACET) or Addition Coupled Electron Coupled Proton Transfer (ACPCET). With a [2.2]paracyclophane-derived biquinone (**1**) as the substrate, the nature of nucleophilic addition onto its sp^2 carbons exhibits a change from stepwise A-ET-PT to ACET-PT and further to ACPCET, in parallel with the decreased nucleophilicity of the attacking reagent. In addition, we further proposed six possible potential energy surfaces and the coupling modes between A, ET and PT, in which three have been found in this work. Quasi-classical trajectory shows that the ACET and PT event can also be dynamically concerted even for an ACET-PT mechanism.

Introduction

Since its first being proposed in 1981¹, the proton coupled electron transfer (PCET) has become a well-known concept, and both its theory²⁻⁷ and practical use⁸⁻¹⁴ have been continuously explored. Under this scheme, besides the Hydrogen Atom Transfer (HAT) reaction, in which both the proton and electron being transferred comes from the same orbital, during the reaction of a hydrogen donor (AH) and an acceptor (B) to give A and BH, there are three possible modes: stepwise electron transfer (ET) to form AH^+ and B^- followed by a proton transfer (PT); stepwise PT affording A^- and BH^+ followed by an ET; and, as called PCET, a concerted proton-electron transfer in one elementary step, especially when single PT or ET is thermodynamically unfavorable. The key point of PCET is that PT and ET can interplay and promote each other: ET leads to increased acidity of the A-H bond, promoting the PT process; at the meantime the negative charge resulted by PT on A further promotes ET. The inter-promoting nature of PT and ET enables their coupling, causing the elementary step of PCET as a result.

The reaction mode possible to couple with ET is not limited to PT. In this work, we focus on another important elementary reaction, namely the nucleophilic addition to electron-deficient olefins (noted as A). The nucleophilic addition reaction toward an olefin substrate is, to some extent, similar to PT from an acidic substrate: both create a partial negative charge which is more prone to be oxidized, and both are activated by a more oxidized (electrophilic) substrate. With a [2.2]paracyclophane-derived biquinone compound **1** (Figure 1) as the model substrate, we studied the impact of nucleophile on the reaction mechanism, and found that the addition reaction can couple with ET and PT, leading to the new elementary reaction of Addition Coupled Electron Transfer (ACET) and Addition Coupled Electron Coupled Proton Transfer (ACPCET).

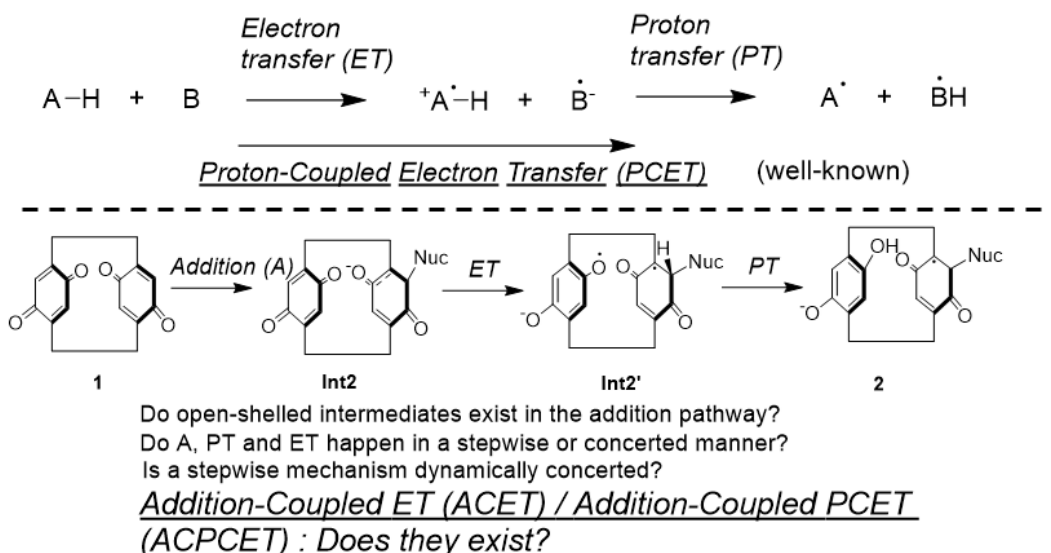


Figure 1. The summary of the concept of PCET, ACET and ACPCET.

Results and Discussions

Initial Insight

Compound **1** has been synthesized and characterized by Staab by oxidizing its phenol precursor in 1973¹⁵. It was chosen as the model substrate in this work, because it bears two quinone rings connected by two short and rigid (CH₂)₂ linkers, enabling short contact of the two reactive rings. As a result, it is of concern that once a nucleophile attacks one quinone ring, leading to an enolate (**Int2** in Figure 1) whether the other quinone ring could act as an intramolecular oxidant to achieve an open-shelled compound **Int2'**. Furthermore, the delicate structure of **1** enables an intramolecular PT from **Int2'** across the two quinone rings, affording the final biradical product **2**. Of interests in this paper is that whether these A, PT, ET processes can efficiently couple, both in terms of minimum energy reaction path (MEP) and reaction dynamics.

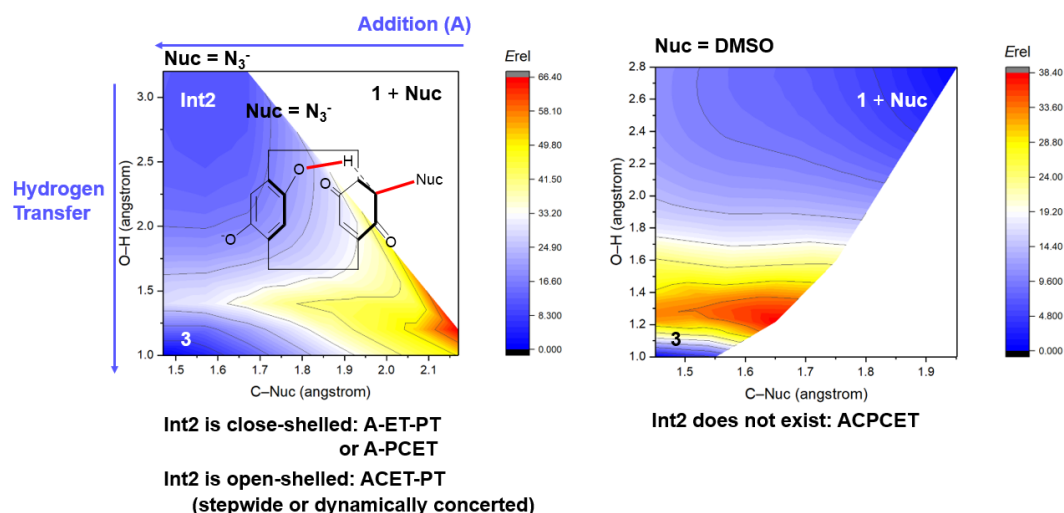


Figure 2. The two-dimensional potential energy contours for the overall A-ET-PT reaction, with N₃⁻ and DMSO as the nucleophile, respectively. Energies are shown in kcal/mol, and the interested bonds are labelled as red.

The first problem of concern is whether the intermediates mentioned in Figure 1 can exist. The answer to this question depends on the nucleophilicity of the attacking reagent. Two typical two-dimensional potential energy surfaces along the reaction coordinate of both addition and hydrogen transfer are shown in Figure 2. On the one hand, for a common nucleophile (Nuc) with enough nucleophilicity, the approaching to **1** leads to a minimum, corresponding to either close-shelled **Int2** or open-shelled **Int2'**. In this case, we expect that a stepwise A-ET-PT or A-PCET or ACET-PT should happen. On the other hand, when the nucleophilicity of Nuc is extremely low, such as Nuc = DMSO, **Int2** and **Int2'** are unable to be a minimum on the potential energy surface, and since **1** is thermodynamically unable to oxidize Nuc to initialize an ET-A-PT process (see Supporting Information), A, ET, PT have to be coupled in one single elementary step, which corresponds to the ACP CET mechanism. In the following part, we separately discuss the three cases: stepwise A-ET-PT; ACET-PT; ACP CET.

Stepwise A-ET-PT when Nuc = Na(THF)₂(OMe) (as noted by NaOMe)

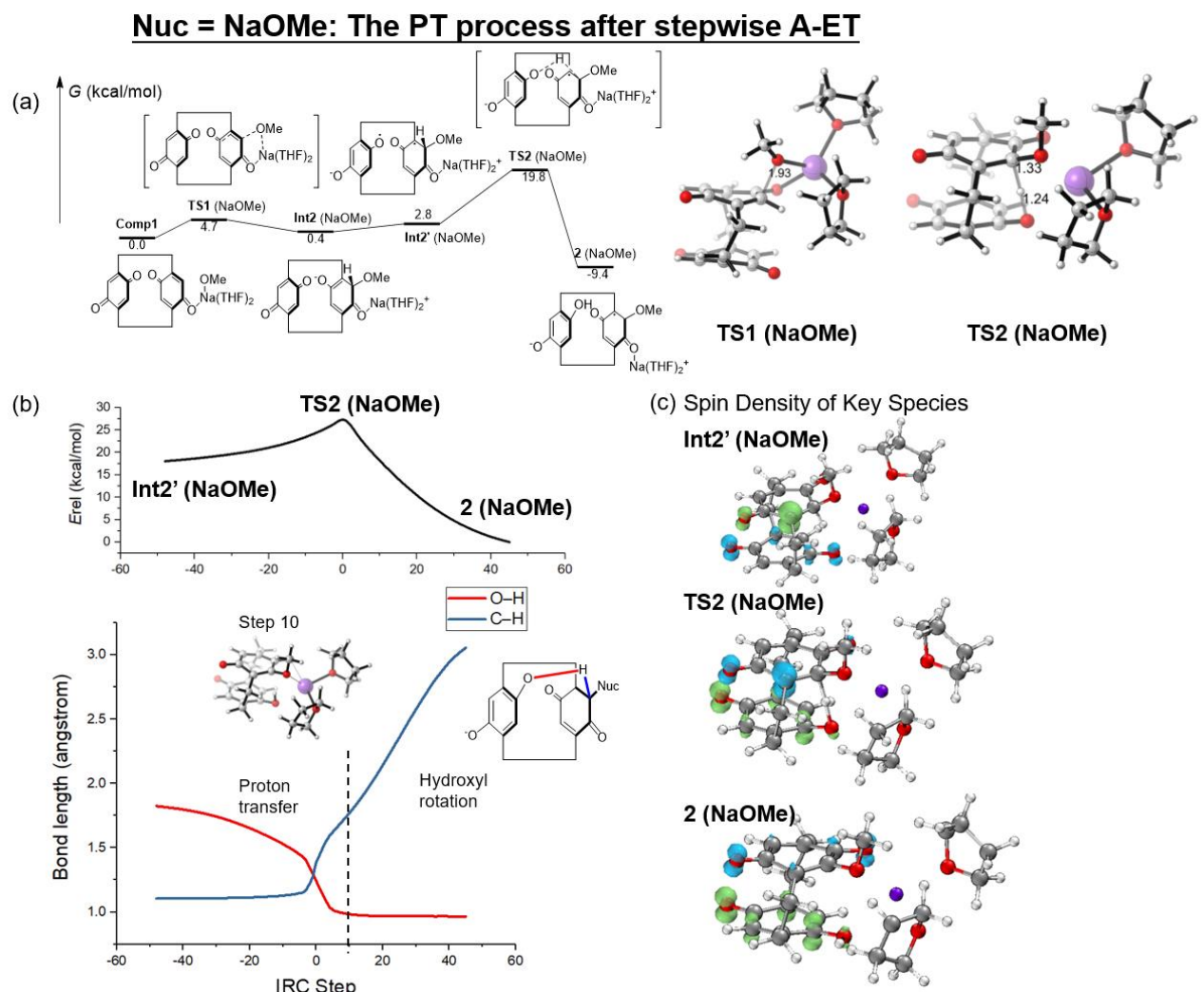


Figure 3. (a) The Gibbs free energy profile for the A-ET-PT reaction with Na(OMe)(THF)₂ (noted as NaOMe) as the nucleophile. (b) the evolution of energy and key bond lengths along the IRC of **TS2(NaOMe)**. (c) The spin density isosurface of the key species.

With NaOMe as Nuc, all the intermediates and transition states in Figure 1 can be located, as shown in Figure 3a. The complex of **1** with NaOMe undergoes a rapid nucleophilic addition with a barrier of 4.7 kcal/mol, affording a close-shelled enolate **Int2** (NaOMe). Then some geometry adjustment occurs, resulting in another minimum on the open-shelled potential energy surface, namely **Int2'**. The spin density isosurface (Figure 3c) shows that an intramolecular ET has happened in **Int2'**, in which, interestingly, the spin density on the quinone ring being attacked localizes on the *ortho*-site of the carbon attacked by Nuc, and the conjugating carbonyl group only shares little spin. On the other hand, the spin density on the ring acting as the oxidant is delocalized over the two carbonyl groups.

After the formation of **Int2'**, an intramolecular PT occurs through **TS2**, with a low barrier of 17.0 kcal/mol. The evolution of the C–H bond being broken and O–H bond being formed along the Intrinsic Reaction Coordinate (IRC) of **TS2** is shown in Figure 3b. The O–H bond slowly decreases to ~1.5 angstrom in the pre-TS region (up to IRC step ~-5), and is sharply shortened to ~1.0 angstrom through **TS2**. The change of C–H bond length is asynchronous with the O–H bond: it almost keeps unchanged at the pre-TS region, undergoes the first increase from IRC step -5 to 10, and then another increase starting from IRC step 10. The two increases correspond to two phases of the overall reaction: the PT phase from IRC point -60 to 10, and then the hydroxyl rotation phase, which can be seen by comparing the geometry of step 10 (Figure 3b) and **2** (NaOMe) (Figure 3c). As for the spin density, all the points along the IRC are open-shelled, indicating that the reaction is almost a simple PT, although spin density at the *ortho*-carbon of both **Int2'** and **TS2** is delocalized onto the two carbonyl groups in the final product **2** at the end of the reaction. According to the observations above: the presence of both **Int2** and **Int2'**, the PT-nature of **TS2**, and the presence of ET in **Int2'**, it is concluded that the overall reaction follows a stepwise A-ET-PT mechanism when NaOMe acts as the Nuc.

ACET-PT when Nuc = Na(THF)₂(OCOCF₃) (as noted by NaTFA)

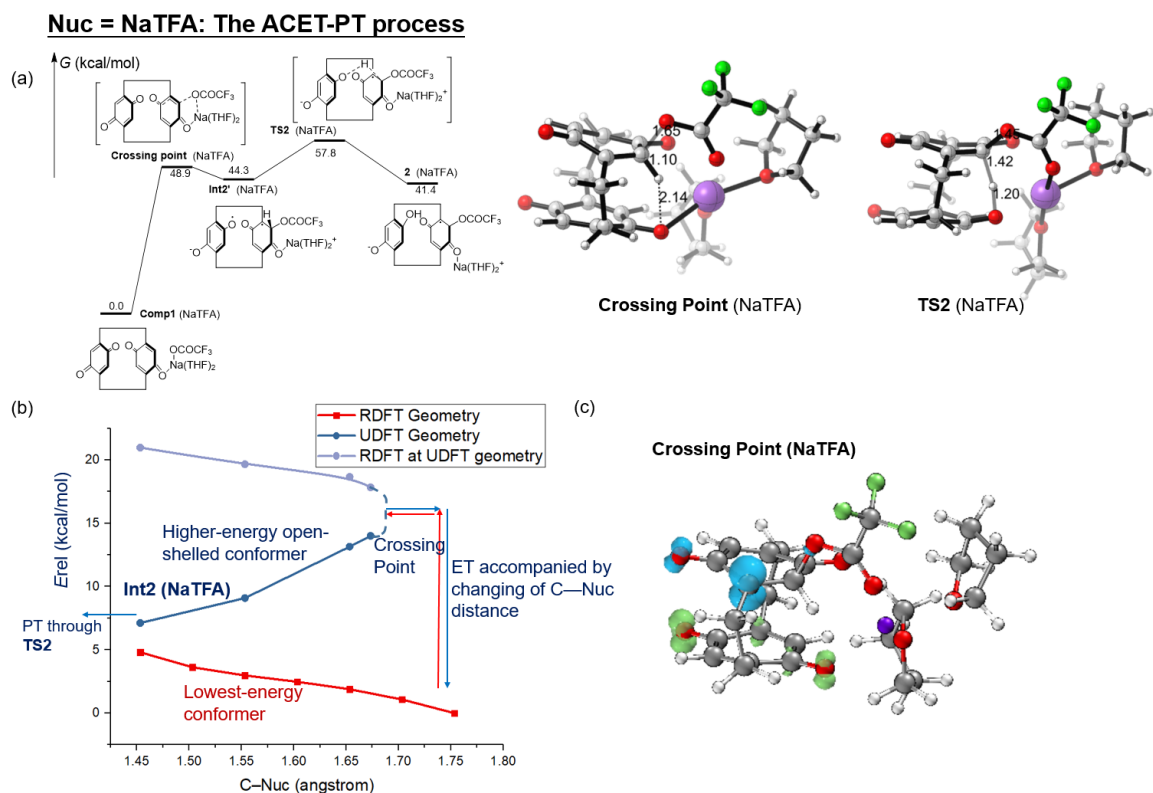


Figure 4. (a) The Gibbs free energy profile for the ACET-PT reaction with Na(THF)₂ (OCOCF₃) (noted as NaTFA) as the nucleophile. (b) The relative energies of the close-shelled (RDFT) and open-shelled biradical (UDFT) conformers with given C–Nuc distance. The line “RDFT at UDFT geometry” was obtained by restricted single point calculation at the geometry of the biradical conformer. (c) The spin density isosurface of the crossing point.

With NaTFA as Nuc, a tetrahedral intermediate-like compound **Int2'** also exists, as the case for NaOMe, although it is much higher in energy (44.3 kcal/mol above the complex form by **1** and NaTFA). The ET-product **Int2'** undergoes PT through **TS2**, with an overall barrier of 57.8 kcal/mol to give the final product **2**. Although the barrier is rather high (notably, there is no minimum corresponding to the addition product with 2,6-dimethyl-1,4-benzoquinone as the substrate, indicating that the ET resulted by the second quinone ring is essential), leading the reaction experimentally inaccessible, it is still theoretically valuable, in providing mechanistic insights into the elementary reaction modes.

Although the formation of **Int2'** and the following PT are similar to the NaOMe case, there is one substantial difference: in the NaTFA case the close-shelled **Int2** is no longer a minimum. By scanning the C–Nuc distance (Figure 4), the energy monotonously increases while Nuc approaches at the close-shelled potential energy surface. It is notable that the biradical compound (as shown by the UDFT geometry in Figure 4b) takes different geometry (see Supporting Information for a graphical visualization of the geometries). Although it is higher in energy than the close-shelled conformer, a minimum (**Int2'**) appears at C–Nuc distance of ~1.45 angstrom. The open-shelled conformer can only exist on the unrestricted DFT (UDFT) surface; once close-shelled restricted DFT (RDFT) is adopted to optimize the geometry at the fixed C–Nuc distance, it is no longer a

minimum, and only the RDFT geometries are able to be located.

By single point calculations with restricted DFT (RDFT), we found that the open-shelled UDFT states are indeed lower than the close-shelled states at the geometry of open-shelled conformers (the line of RDFT at UDFT geometry in Figure 4b). The energy difference of RDFT and UDFT single point calculations decreases as the C–Nuc bond stretches, and finally a crossing point is expected to be met. Unfortunately, accurate locating of the crossing point is extremely hard because the UDFT conformer “collapses” onto the RDFT potential energy surface once C–Nuc distance is longer than 1.67 angstrom. Therefore, we have to take the UDFT geometry with C–Nuc fixed at 1.67 angstrom as an approximation of the crossing point. Despite the presence of one single imaginary frequency corresponding to the C–Nuc stretching vibration, it is not a transition state because of its non-zero gradient. The crossing point exhibits similar spin density distribution to **Int2'**, indicating that an ET event occurs at this point, and only then a minimum can be formed. By other words, it can be considered that the ET from the close-shelled conformer leads directly to not a minimum of the “ET product”, but the crossing point that directly connects the product of both ET and addition (**Int2'**), and thus in this case the addition and ET are coupled in one elementary step (ACET). The difference between ACET and stepwise ET-A-PT will be further discussed in the later section.

ACPCET when Nuc = DMSO

Nuc = DMSO: the ACPCET process

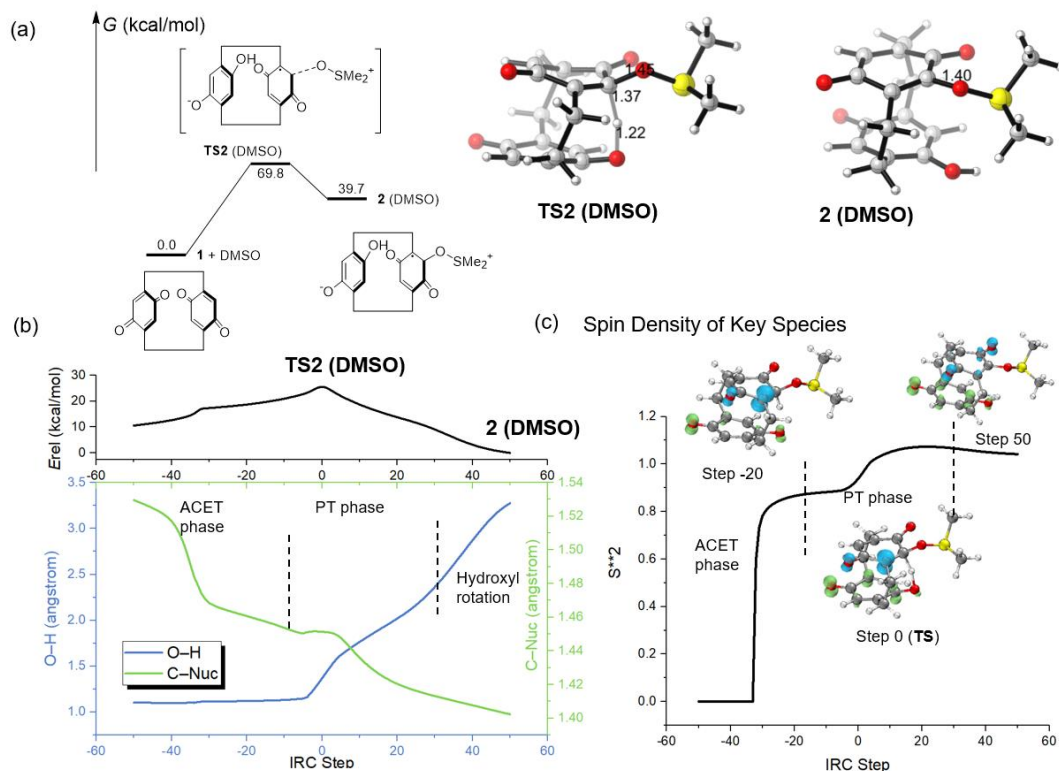


Figure 5. (a) The Gibbs free energy profile for the ACPCET reaction with DMSO (noted as NaTFA) as the nucleophile. (b) The evolution of key bond lengths along the IRC of **TS2 (DMSO)**. (c) The S^{*2} along the IRC, and spin density isosurface of selected points

As compared with NaTFA, DMSO is an even weaker Nuc, as reflected by its higher addition barrier (**TS2** in Figure 5a) of 69.8 kcal/mol, and absence of both **Int2** and **Int2'** (Figure 2). The overall A-PT-ET process proceeds through only one transition state **TS2** (DMSO). The IRC profile of **TS2** (DMSO) can be divided into three stages: the approaching of DMSO to the substrate carbon atom accompanied by ET (the ACET phase, up to step -10 in Figure 5b), the PT phase (from step 10 to ~30), and the hydroxyl rotation phase. The complex remains close-shelled at the beginning of the addition phase, as seen by the S^{**2} of zero in Figure 5c; at step ~-30, however, the ET event suddenly occurs, giving a S^{**2} of ~0.8. Then the nucleophile continues approaching the substrate, although with a less slope, until it reaches ~step -10, where the PT process starts according to the decreasing O–H distance. Notably, although they are divided into different phases in order to magnify the asynchronicity of PT with ACET, the C–Nuc distance keeps decreasing after a short platform period in the PT phase, and finally reaches 1.40 angstrom in **2** (DMSO). The evolution of spin density along IRC shares a similar mode with the stepwise mechanism: first close-shelled, then ET event occurs although coupled with other bond formation and the *ortho*-carbon to the carbon being attacked accumulates spin, and finally the spin is delocalized onto all the carbonyl groups in **2**.

To Distinguish the Mechanisms

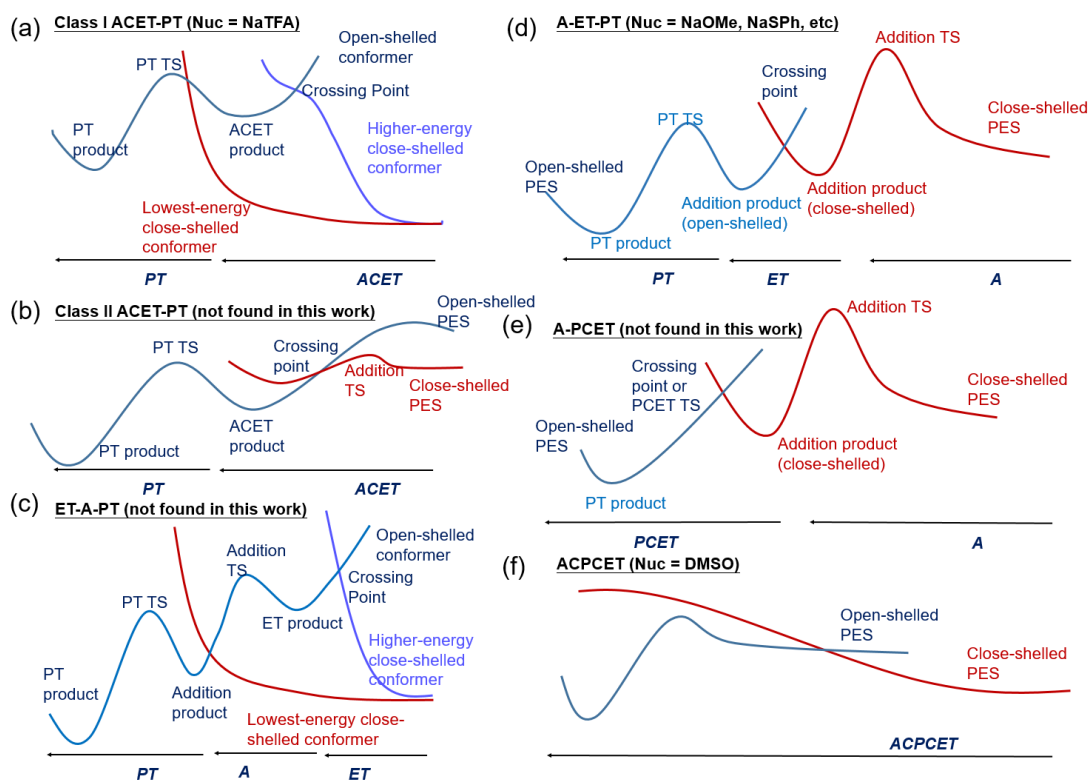


Figure 6. The schematic potential energy surface for the possible coupling modes among the A, ET, PT reactions.

Up to now, we have discussed three examples with different coupling modes among A, ET, PT. In order to further clarify their relationship, the schematic models of their potential energy surfaces

are plotted in Figure 6. Consider the crossing between the close-shelled and open-shelled potential energy surfaces: in the presence of a strong nucleophile, the addition product **Int2** is able to be a minimum on the close-shelled surface. In this regard, if the crossing point occurs later than its formation, and the resulted ET-product, namely open-shelled addition product **Int2'** is also a minimum, then the reaction goes through two transition states divided by one crossing point, affording a typical stepwise A-ET-PT process (Figure 6d). If the ET product **Int2'** is not a minimum, and directly leads to the product **2**, then it follows an A-PCET mechanism (Figure 6e). On the other hand, if the crossing point appears earlier than the formation of **Int2**, an ET event should happen at the post-TS region of addition, and directly connects with the ACET product (Class II ACET, Figure 6b).

If the nucleophile is too weak to form a close-shelled addition product **Int2** as a minimum, then we go the cases of Figure 6a, 6c and 6f. The difference between ET-A-PT and Class I ACET-PT relies on whether the “pure” ET product (namely 1^- and Nuc^+) is able to exist as a minimum on the open-shelled surface; if a minimum is formed, then a barrier has to be overcome for addition, then a stepwise ET-A-PT reaction occurs (Figure 6c). However, in the $\text{Nuc} = \text{NaTFA}$ case, there is no such ET product (see Table S1 for the redox potential), and thus no addition TS on the open-shelled surface. Instead, after the ET event through the crossing point, the addition product with electron transferred is directly obtained, which is classified as the Class I ACET (Figure 6a). If even the ACET product **Int2'** cannot exist as a minimum, as seen for $\text{Nuc} = \text{DMSO}$ case, only one transition state appears along the whole reaction, and gives a fully coupled ACPCET reaction (Figure 6f).

Quasiclassical Molecular Dynamics Simulation

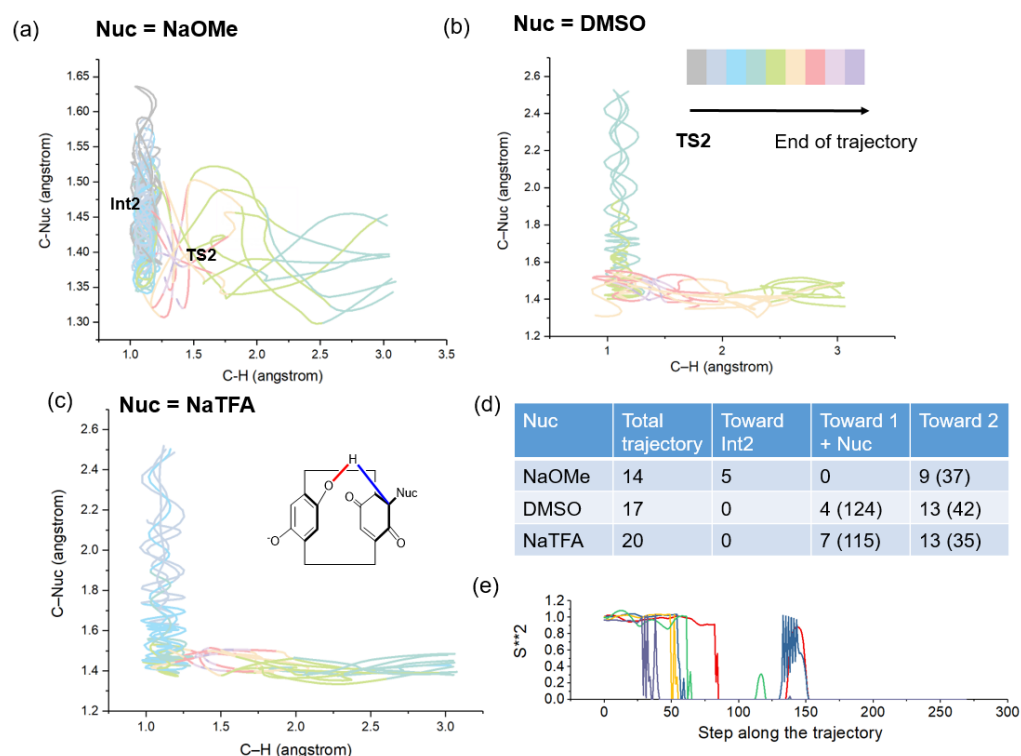


Figure 7. (a-c) The evolution of interested bond lengths along the trajectories initiated from **TS2** with various nucleophiles. (d) The numbers of trajectories leading to each outcome. The average timing (fs) is shown in parenthesis. (e) The S^{**2} along the trajectories leading to **Int2** (NaOMe) from **TS2** (NaOMe).

In order to further study the coupling among each step in real reaction, quasi-classical molecular dynamics trajectories were initiated from **TS2** and the evolution of key bond lengths was recorded. For all the three nucleophiles, recrossing is quite common, as seen by the nearly doubled number of the trajectories leading to **2** over to **Int2** or separated **1** + Nuc. The PT event happens rapidly in ~ 40 fs, regardless of the nucleophile. However, the fate of the trajectories toward the direction of **Int2** (or **Int2'**) is relevant to the nucleophile. On the one hand, for NaOMe, 5 out of the 14 trajectories leads to close-shelled **Int2**, which is stable in the time period of 300 fs. The evolution of S^{**2} for each point (Figure 7e) suggested that the complex returned to be close-shelled in almost ~ 50 fs, and then the system oscillates between **Int2** ($S^{**2} = 0$) and **Int2'** ($S^{**2} \sim 0.8$, appears near ~ 150 fs). On the other hand, no **Int2** or **Int2'** appears with adequate stability in the trajectories, and all the trajectories running toward their direction lead to dissociated **1** and Nuc in a similar timing of ~ 120 fs for NaTFA and DMSO. As a result, although they follow the ACET-PT and ACP CET mechanistic pattern respectively, dynamically they behave similarly: **Int2'** is not a “dynamically stable” intermediate, and the ACET and PT events are dynamically concerted in the NaTFA case.

Conclusion

According to the discussions above, based on potential energy scan, IRC analysis and quasiclassical molecular dynamics, we have suggested the reaction mode of ACET and ACP CET, in which the addition, proton transfer and electron transfer effectively couple in one elementary step. With the [2.2]paracyclophane-derived biquinone **1** as the model substrate, we have shown that the mechanism of nucleophilic addition onto its sp^2 carbon exhibits a consecutive change from stepwise A-ET-PT to ACET-PT and finally to ACP CET. The coupling of A with ET and PT is in consistence with the order of nucleophilicity: when the nucleophile is strong, a stepwise A-ET-PT occurs; otherwise, with an adequately weak nucleophile, the ACET-PT, ACP CET, or other coupling modes has to occur to compensate the unfavorable addition, and which of them occurs depends on the shape of potential energy surface, as shown in Figure 6. Besides, quasiclassical trajectories show that these steps can be dynamically concerted, even when they seem to be stepwise according to the potential energy surface.

Although the examples of ACET and ACP CET in this work are of extremely high barrier, we believe that there exist other systems that ACET and ACP CET process is able to occur under experimentally accessible condition. For example, before submitting this work, we saw Fujii's latest report¹⁶ on the electron-coupled epoxidation reaction of olefin, with should be another example of ACET. Also, we believe that the remaining three types of coupling not discussed in this work, namely Class II ACET, A-PCET and ET-A-PT, can also be found in the future.

Methods

The Gaussian 16 package¹⁷ was employed to perform all the calculations, with the Gaussian 09 default integral grid. The wB97x-D functional¹⁸ was used for all calculations. For geometry

optimization, the def2-SVP¹⁹ basis set was employed. Frequency calculations were followed to ensure stationary points were found, and to obtain Gibbs free energy correction at room temperature. Single point calculations were performed with the def2-TZVPP basis set. Both geometry optimization and single point calculation were performed under SMD implicit solvation²⁰ of THF. The stability of wavefunction was checked for all the structures.

The spin density analysis were performed with the Multiwfn program²¹. The molecular geometry and isosurface were plotted with CYLView²² and VMD²³.

The quasiclassical trajectory molecular dynamics simulations were performed using the PROGDYN program²⁴. The initial geometry for each trajectory was generated by adding displacements that follows a QM-like Gaussian distribution to all vibrational modes higher than 10 cm⁻¹ of **TS2**. Each real normal mode was given its zero-point energy plus a random Boltzmann sampling of the thermal energy available at 298.15 K. Trajectories were propagated at wB97x-D/def2-SVP/SMD(THF) level in both the forward and backward directions, until the product formed or the length of trajectory is longer than 300 fs.

Acknowledgement

Yumiao Ma thanks Hangzhou Yanqu Information Technology Co., Ltd for purchasing the license for Gaussian. Also thanks to all the students in Department of Chemistry, Tsinghua University, for their great love and encouragement toward Ma. Besides, Ma wants to mention a friend Zongchang Han (Tsinghua University); although he does not contribute in this work, he happened to have the concept of ACET in his independent project in 2018, although ACET did not occur in his project. In other words, Han has the idea of ACET earlier than Ma.

References:

1. Binstead, R. A.; Moyer, B. A.; Samuels, G. J.; Meyer, T. J., Proton-coupled electron transfer between [Ru (bpy) 2 (py) OH2] 2+ and [Ru (bpy) 2 (py) O] 2+. A solvent isotope effect (kH2O/kD2O) of 16.1. *Journal of the American Chemical Society* **1981**, *103* (10), 2897-2899.
2. Huynh, M. H. V.; Meyer, T. J., Proton-coupled electron transfer. *Chemical Reviews* **2007**, *107* (11), 5004-5064.
3. Mayer, J. M., Proton-coupled electron transfer: a reaction chemist's view. *Annu. Rev. Phys. Chem.* **2004**, *55*, 363-390.
4. Migliore, A.; Polizzi, N. F.; Therien, M. J.; Beratan, D. N., Biochemistry and theory of proton-coupled electron transfer. *Chemical reviews* **2014**, *114* (7), 3381-3465.
5. Tyburski, R.; Liu, T.; Glover, S. D.; Hammarström, L., Proton-Coupled Electron Transfer Guidelines, Fair and Square. *Journal of the American Chemical Society* **2021**, *143* (2), 560-576.
6. Warren, J. J.; Tronic, T. A.; Mayer, J. M., Thermochemistry of proton-coupled electron transfer reagents and its implications. *Chemical reviews* **2010**, *110* (12), 6961-7001.
7. Weinberg, D. R.; Gagliardi, C. J.; Hull, J. F.; Murphy, C. F.; Kent, C. A.; Westlake, B. C.; Paul, A.; Ess, D. H.; McCafferty, D. G.; Meyer, T. J., Proton-coupled electron transfer. *Chemical Reviews* **2012**, *112* (7), 4016-4093.
8. Bruch, Q. J.; Connor, G. P.; Chen, C.-H.; Holland, P. L.; Mayer, J. M.; Hasanayn, F.; Miller, A. J., Dinitrogen Reduction to Ammonium at Rhenium Utilizing Light and Proton-Coupled Electron Transfer. *Journal of the American Chemical Society* **2019**, *141* (51), 20198-20208.

9. Gentry, E. C.; Knowles, R. R., Synthetic applications of proton-coupled electron transfer. *Accounts of chemical research* **2016**, *49* (8), 1546-1556.
10. Huang, L.; Ji, T.; Rueping, M., Remote Nickel-catalyzed cross-coupling arylation via proton-coupled electron transfer-enabled C–C bond cleavage. *Journal of the American Chemical Society* **2020**, *142* (7), 3532-3539.
11. Lehnher, D.; Lam, Y.-h.; Nicasri, M. C.; Liu, J.; Newman, J. A.; Regalado, E. L.; DiRocco, D. A.; Rovis, T., Electrochemical synthesis of hindered primary and secondary amines via proton-coupled electron transfer. *Journal of the American Chemical Society* **2019**, *142* (1), 468-478.
12. Mora, S. J.; Odella, E.; Moore, G. F.; Gust, D.; Moore, T. A.; Moore, A. L., Proton-coupled electron transfer in artificial photosynthetic systems. *Accounts of chemical research* **2018**, *51* (2), 445-453.
13. Roos, C. B.; Demaerel, J.; Graff, D. E.; Knowles, R. R., Enantioselective hydroamination of alkenes with sulfonamides enabled by proton-coupled electron transfer. *Journal of the American Chemical Society* **2020**, *142* (13), 5974-5979.
14. Zhao, K.; Yamashita, K.; Carpenter, J. E.; Sherwood, T. C.; Ewing, W. R.; Cheng, P. T.; Knowles, R. R., Catalytic ring expansions of cyclic alcohols enabled by proton-coupled electron transfer. *Journal of the American Chemical Society* **2019**, *141* (22), 8752-8757.
15. Rebařka, W.; Staab, H. A., Ein „intramolekulares Chinhydron“ . *Angewandte Chemie* **1973**, *85* (18), 831-832.
16. Ishimizu, Y.; Ma, Z.; Hada, M.; Fujii, H., Rate-Limiting Step of Epoxidation Reaction of the Oxoiron(IV) Porphyrin π -Cation Radical Complex: Electron Transfer Coupled Bond Formation Mechanism. *Inorganic Chemistry* **2021**.
17. Frisch, M. J.; Trucks, G. W.; Schlegel, H. B.; Scuseria, G. E.; Robb, M. A.; Cheeseman, J. R.; Scalmani, G.; Barone, V.; Petersson, G. A.; Nakatsuji, H.; Li, X.; Caricato, M.; Marenich, A. V.; Bloino, J.; Janesko, B. G.; Gomperts, R.; Mennucci, B.; Hratchian, H. P.; Ortiz, J. V.; Izmaylov, A. F.; Sonnenberg, J. L.; Williams, D.; Ding, F.; Lipparini, F.; Egidi, F.; Goings, J.; Peng, B.; Petrone, A.; Henderson, T.; Ranasinghe, D.; Zakrzewski, V. G.; Gao, J.; Rega, N.; Zheng, G.; Liang, W.; Hada, M.; Ehara, M.; Toyota, K.; Fukuda, R.; Hasegawa, J.; Ishida, M.; Nakajima, T.; Honda, Y.; Kitao, O.; Nakai, H.; Vreven, T.; Throssell, K.; Montgomery Jr., J. A.; Peralta, J. E.; Ogliaro, F.; Bearpark, M. J.; Heyd, J. J.; Brothers, E. N.; Kudin, K. N.; Staroverov, V. N.; Keith, T. A.; Kobayashi, R.; Normand, J.; Raghavachari, K.; Rendell, A. P.; Burant, J. C.; Iyengar, S. S.; Tomasi, J.; Cossi, M.; Millam, J. M.; Klene, M.; Adamo, C.; Cammi, R.; Ochterski, J. W.; Martin, R. L.; Morokuma, K.; Farkas, O.; Foresman, J. B.; Fox, D. J. *Gaussian 16 Rev. C.01*, Wallingford, CT, 2016.
18. Chai, J.-D.; Head-Gordon, M., Long-range corrected hybrid density functionals with damped atom-atom dispersion corrections. *Physical Chemistry Chemical Physics* **2008**, *10* (44), 6615-6620.
19. Weigend, F.; Ahlrichs, R., Balanced basis sets of split valence, triple zeta valence and quadruple zeta valence quality for H to Rn: Design and assessment of accuracy. *Physical Chemistry Chemical Physics* **2005**, *7* (18), 3297-3305.
20. Marenich, A. V.; Cramer, C. J.; Truhlar, D. G., Universal solvation model based on solute electron density and on a continuum model of the solvent defined by the bulk dielectric constant and atomic surface tensions. *The Journal of Physical Chemistry B* **2009**, *113* (18), 6378-6396.
21. Lu, T.; Chen, F., Multiwfn: a multifunctional wavefunction analyzer. *Journal of computational chemistry* **2012**, *33* (5), 580-592.
22. Legault, C., CYLview, 1.0 b. *Université de Sherbrooke* **2009**, 436, 437.
23. Humphrey, W.; Dalke, A.; Schulten, K., VMD: visual molecular dynamics. *Journal of molecular*

graphics **1996**, *14* (1), 33-38.

24. Singleton, D. A.; Hang, C.; Szymanski, M. J.; Greenwald, E. E., A New Form of Kinetic Isotope Effect. Dynamic Effects on Isotopic Selectivity and Regioselectivity. *Journal of the American Chemical Society* **2003**, *125* (5), 1176-1177.